PHYSICAL REVIEW A

STATISTICAL PHYSICS, PLASMAS, FLUIDS, AND RELATED INTERDISCIPLINARY TOPICS

THIRD SERIES, VOLUME 43, NUMBER 12 15 JUNE 1991

Universal conductivity curve for a plane containing random holes

E. J. Garboczi
National Institute of Standards and Technology, Building Materials Division, 226/B348, Gaithersburg, Maryland 20899

M. F. Thorpe and M. S. DeVries
Department of Physics and Astronomy, Michigan State University, East Lansing, Michigan 48824

A. R. Day
Department of Physics, Marquette University, Milwaukee, Wisconsin 53233
(Received 2 January 1991)

This paper examines the general percolation problem of cutting randomly centered insulating holes in a two-dimensional conducting sheet, and explores how the electrical conductivity σ decreases with the remaining area fraction. This problem has been studied in the past for circular, square, and needlelike holes, using both computer simulations and analog experiments. In this paper, we extend these studies by examining cases where the insulating hole is of arbitrary shape, using digital-image-based numerical techniques in conjunction with the Y-∇ algorithm. We find that, within computational uncertainty, the scaled percolation threshold, $x_c = n_c \langle L_{\rm eff}^2 \rangle = 5.9 \pm 0.4$, is a universal quantity for all the cases studied, where n_c is the critical value at percolation of the number of holes per unit area n, and $\langle L_{\rm eff}^2 \rangle$ is a measure of n_I^{-1}, the initial slope of the $\sigma(n)$ curve, calculated in the few-hole limit and averaged over the different shapes and sizes of the holes used. For elliptical holes, $L_{\rm eff} = 2(a+b)$, where a and b are the semimajor and semiminor axes, respectively. All results are well described by the universal conductivity curve: $\sigma/\sigma_0 = [(1-x/5.90)(1+x/5.90-x^2/24.97)(1+x/3.31)^{-1}]^{1.3}$, where $x = nL_{\rm eff}^2$, and σ_0 is the conductivity of the sheet before any holes are introduced.

I. INTRODUCTION

The problem studied in this paper is that of the conductivity of a random continuum. We start with a uniform two-dimensional sheet of host-conducting material with conductivity σ_0, and randomly introduce extended defects having conductivity σ_d and some given shape. These defects are allowed to freely overlap. When σ_d is nonzero, we have a composite material. When σ_d is zero, the defect is thought of as a hole, resulting in a continuum percolation problem. In this case, p denotes the area fraction of σ_0 material remaining after a given number of defects have been introduced, or holes punched out.

In recent years, much attention has been given to the value of critical exponents at the percolation threshold. For the conductance case, the exponent of interest, usually denoted by t, determines how the conductance goes to zero at $p = p_c$, the critical threshold. In this paper, we concentrate on two subjects that are arguably of more importance in the kind of continuum percolation problems that arise in real materials: (1) the overall behavior of the conductance as a function of p, and (2) the relationship between the effect of one defect on the overall conductivity and the many-defect critical threshold.

Previous work on which this present effort builds includes a joint experimental and computer simulation study of the continuum percolation problem of needle-shaped insulating defects,[1] hereafter referred to as I, and a study of the dependence of the percolation threshold on the aspect ratio of the elliptical holes introduced,[2] denoted hereafter as II.

In Sec. II we briefly review previous efforts to relate one-defect properties with percolation thresholds, which have been mainly cast as attempts to formulate a dimensionless, invariant percolation threshold using lengths or areas that are definable by one-defect properties only. In Sec. III, we present new computer simulations for the needle problem, using both continuum and lattice techniques. We define the initial slope and critical threshold of the needle problem in terms of the number of defects per unit area and use this to define a generalized dimensionless variable that is natural for this problem and that suggests the invariant defined in this paper. Ellipse percolation threshold data from II is used as a first test of

the new invariant in Sec. IV. Section V presents digital-image simulations of percolation problems with arbitrarily shaped defects. We show that the critical concentration of defects can be predicted from knowledge of the conductivity in the few-defect limit without even knowing the shape of the defects. In Sec. VI we define a universal conductivity curve for the class of percolation problems described in this paper. It is shown that all previous conductivity data, both from simulations and experiments, falls on this universal conductivity curve. In the summary, we discuss how the universal conductivity curve should be used.

II. DIMENSIONAL INVARIANTS FOR PERCOLATION THRESHOLDS

Looking at the percolation literature as a whole, there are two main bodies of work. The first is produced by those researchers who are interested in the percolation phase transition as a model second-order phase transition. The focus of their work is on the various critical exponents displayed as p approaches its critical value p_c either from above or below, and the interrelations between these critical exponents.

The second body of work is produced by those who are more interested in applications of percolation geometry to real materials problems. These researchers tend to focus on the value of p_c as a function of material microstructure, as the mere existence of a percolation threshold is what tends to dominate material properties, rather than the exact values of the critical exponents.

Most theoretical progress seems to have been made in the first area above, that of critical exponents and their interrelationships. Good reviews of percolation critical properties exist.[3] Our work, however, deals with the latter category, that of relating p_c to microstructure via invariants constructed out of p_c and properties of microstructural constituents.

The first work in this area was done by Scher and Zallen[4,5] in 1970. They proposed, for site percolation problems on a lattice, that p_c, the critical fraction of sites present, would be an invariant when expressed as a volume fraction, depending only on dimensionality. Their construction was to center a sphere, with radius equal to half the nearest-neighbor lattice spacing d, at each site. The critical volume fraction occupied, $a_c \equiv p_c \pi d^2/(4a_{\text{prim}}) = 0.45$ in two dimensions, and $v_c \equiv p_c \pi d^3/(6v_{\text{prim}}) = 0.16$ in three dimensions, was then found to be invariant, within 10% or less, for regular and irregular lattices,[5] where a_{prim} and v_{prim} are the primitive site volumes for the lattices considered. This invariant seems to hold only for percolation clusters built up of nonoverlapping particles, since, for example, in two dimensions, overlapping circles with random centers require a higher area coverage of 0.68 in order to percolate.[6] Recently, in a lattice-based growth model for the reactive growth during curing of cement-based materials, percolation thresholds for solid and pore phases were found to roughly agree, in two and three dimensions, with the Scher and Zallen invariants.[7,8] Thus there are some complex percolation problems to which the Scher and Zallen conjecture is relevant, although the precise conditions necessary for this conjecture to hold are not yet clear.

For continuum percolation problems, with overlapping defects, for which the Scher and Zallen conjecture is definitely not applicable, the main work on predicting p_c has been by Balberg and co-workers.[9] The focus of their work has been on using the excluded volume or area to construct invariants with which to predict p_c, in problems where randomly centered defects like circles and rods are introduced into a host material, gradually culminating in a percolation transition.

The excluded volume of an object is that volume of space around the object in which the center of another such object can be placed so as to guarantee an overlap. For example, for a circle in two dimensions, the excluded area a_{ex} is $4\pi r^2$, since two circles with radius r whose centers are less than $2r$ apart must overlap. In general, if the objects have a size or orientation distribution, one defines $\langle a_{\text{ex}} \rangle$ or $\langle v_{\text{ex}} \rangle$, the local excluded area or volume averaged over these distributions, so that the total excluded area or volume at percolation is $\langle A_{\text{ex}} \rangle = n_c \langle a_{\text{ex}} \rangle$ or $\langle V_{\text{ex}} \rangle = n_c \langle v_{\text{ex}} \rangle$, where n_c is the percolation threshold defined in terms of a critical number of objects per unit area.

References 9 and 10 summarize in more detail what is known about the proposed invariants $\langle V_{\text{ex}} \rangle$ and $\langle A_{\text{ex}} \rangle$. The following two results are known: (1) the critical excluded volume is a dimensional invariant for continuum systems where the defects are all of the same shape and orientation (circles or parallel squares with various size distributions), and (2) when random orientations of the defects are allowed, then the critical excluded volume is much more variable. Even though the critical excluded volume is not the same for cases (1) and (2), it can be approximately bounded[10] by $3.2 < \langle A_{\text{ex}} \rangle < 4.5$, and $0.7 < \langle V_{\text{ex}} \rangle < 2.8$.

In Sec. IV, a better invariant is described that is the *same* for *both* cases (1) and (2) above.

III. NEEDLE SIMULATION RESULTS

In I, the continuum percolation-conduction problem of a conducting sheet with random insulating needle-shaped holes was studied, both experimentally and using computer simulation. The applied voltage is always in the horizontal direction. The needles were equal length, zero-width cuts through which no electrical current could flow.

The experimental study was carried out using needles that were aligned horizontally or vertically with equal probability, and placed with random centers throughout the conducting sheet. Because of the experimental method used, the needles were actually very thin rectangles, with a width to length ratio of about 50. Periodic boundary conditions were not employed. A needle whose center would fall outside the sheet boundary was not allowed to be placed. However, there were many needles, with centers near the boundary, which when placed overlapped the boundary. More experimental details are

given in I.

Computer simulations for the electrical conductivity were carried out using the "blind-ant" algorithm.[11] A random array of horizontal and vertical needles was created, using periodic boundary conditions, and then many random walkers, called ants, were "parachuted" down onto the sheet at random positions, and made to carry out random walks in the open areas, with the restriction that the ants could not cross a needle. The blind-ant results presented in this paper represent improvements on the work described in I. The algorithm used incorporated the first passage method of Tobochnik,[12] whenever the walker was farther away than a predetermined distance from the nearest needle. We also used a variable step length in the random walk to allow for the possibility of passing through arbitrarily small "necks" between needles. The correlations length ξ was computed from the mean-squared radius of gyration of the needle clusters, and was found to be a good fit to the formula $\xi^2/L^2=(1-n/n_c)^{-8/3}/12$. For each ant, the number of steps was chosen so that the mean-squared distance covered was $(5\xi)^2$ from the starting point.

A lattice computation was also carried out for this problem. A square lattice with $N-1$ rows and N columns of conductors was set up, with the first and last column of conductors set to infinite conductivity to serve as the electrodes. This is the arrangement needed to ensure a unit conductivity for the entire lattice, and is convenient for the implementation of the Y-∇ conductivity algorithm.[13] To place a needle, the appropriate bonds are simply removed. A horizontal needle is represented by removing a line of vertical bonds and vice versa for a vertical needle. When the desired number of needles were placed, the Y-∇ algorithm was used to compute the new effective conductivity. The well-documented speed of this algorithm[13] enabled large ($N=1000$) lattices to be used, which gave an acceptable degree of resolution in the lattice representation of the continuum needle problem. The needle length used was $L=20$ lattice spacings.

Since needles have zero width and thus zero area, the usual remaining area fraction variable p cannot be used, and so we switch to the variable n, which is the number of needles per unit area. The percolation threshold is then denoted n_c, and the initial slope of the conductivity versus n curve, which is defined for a single needle, is conveniently quantified as n_I, where n_I is the point on the n axis at which the conductivity curve would extrapolate to zero, if the conductivity continued to follow the initial slope.

Again taking the applied voltage to be in the horizontal direction, then the conductivities σ^H and σ^V for a few horizontal or vertical elliptical holes in a sheet with conductivity σ_0 are

$$\sigma^H/\sigma_0=1-n\pi b(a+b)$$
and
$$\sigma^V/\sigma_0=1-n\pi a(a+b)\ , \tag{1}$$

where a horizontal ellipse means that the semimajor axis a is aligned in the horizontal direction. Averaging the pair of equations shown in Eq. (1) gives the result

$$\sigma/\sigma_0=1-n\pi(a+b)^2/2\equiv 1-n/n_I\ , \tag{2}$$

which requires n_I to be defined by

$$n_I[2(a+b)]^2=8/\pi\ , \tag{3}$$

where a and b are the semimajor and semiminor axes of the elliptical hole. When b goes to zero, we have the needle result that

$$x_I\equiv n_I L^2=8/\pi\ , \tag{4}$$

where $L=2a$ is the length of the needle. For a few vertical-only needles, Eq. (4) changes to

$$x_I=n_I L^2=4/\pi\ . \tag{5}$$

The results in Eqs. (1)–(5) are exact. In the lattice approach to the needle problem, however, since the end of a needle is not well defined, one must examine the computed initial slope to see how the nominal length L of a needle, in terms of how many bonds are removed, compares to the length that is defined by the computed slope. We simulated a single vertical needle in a 1000×999 lattice by removing a column of L horizontal bonds, and computing the new conductivity via the Y-∇ algorithm (approximately two hours of CPU time on a Cyber 205). It turns out that for any L, the conductivity is reduced slightly more by a lattice needle than the continuum result predicts. This difference is due to the finite resolution of the lattice, and can be interpreted in one of two ways. We can either say that the lattice imparts a finite thickness to the needle, and so think of the lattice needle as an effective ellipse, or we can assume the lattice needle is a true zero-width needle, but with an effective length $L_{\rm eff}$ slightly longer than L. The former interpretation is inconsistent with the fact that a single horizontal needle on the lattice does not change the conductivity, and so does act like a true zero-width needle. The latter interpretation, however, will only be useful if the difference between $L_{\rm eff}$ and L is independent of L, for reasonable values of L. Figure 1 shows $\delta L\equiv L_{\rm eff}-L$ plotted against L, with $1<L<40$. $L_{\rm eff}$ is defined using Eq. (5) by equat-

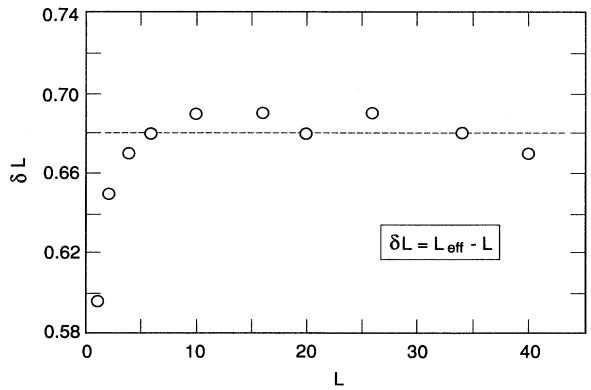

FIG. 1. Showing $\delta L=L_{\rm eff}-L$ for insulating needles on a lattice. L is the nominal length, and $L_{\rm eff}$ is the effective length determined electrically. After $L=6$, the graph asymptotes to $\delta L=0.68$.

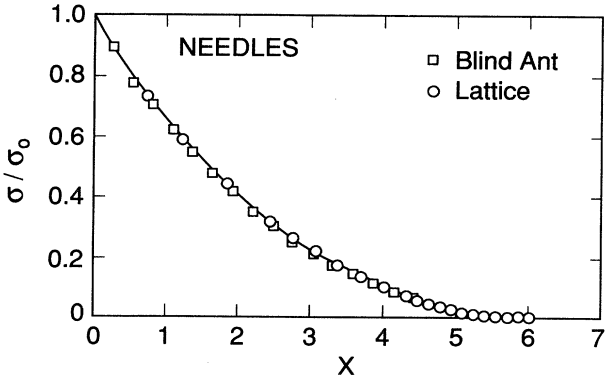

FIG. 2. Showing the conductivity vs $x=nL_{\text{eff}}^2$ data for needles. The squares are improved blind-ant data, and the circles are the lattice simulation data points. The appropriate L_{eff} for each method is discussed in the text. The solid line is the universal conductivity curve (15).

ing the computed lattice result for n_I to $4/\pi L_{\text{eff}}^2$. It is clear that for all $L \geq 6$, δL is approximately equal to the constant value of 0.68. The data point at $L=1$ is just the exact single-bond-defect result,[14] $\delta L=\sqrt{8/\pi}=0.596$. It is therefore valid to think of the lattice needle electrically as a true continuum needle, but with an effective length $L_{\text{eff}}=L+0.68$ (in units of lattice spacings) for $L \geq 6$.

Figure 2 displays the blind-ant and lattice results plotted against the variable $x=nL_{\text{eff}}^2$, with $L_{\text{eff}}=L$ for the blind-ant simulation, and $L_{\text{eff}}=L+0.68$ for the lattice simulation. This variable makes the initial slopes of the two sets of data the same. The solid line is the universal conductivity curve to be discussed in Sec. VI.

It was not possible to extend the blind-ant algorithm beyond $n/n_c=0.8$, as the CPU time required to transverse 5ξ became too long. For this reason, the results for the blind-ant algorithm for $n/n_c \geq 0.8$ are omitted from Fig. 2.

The value of $x_c=n_cL_{\text{eff}}^2$, where the appropriate L_{eff} was used, differs somewhat for different methods. The lattice result, for 40 configurations of $L=20$ needles on a 1000×999 lattice, was 5.7 ± 0.2. Other results from the literature include 5.7 (for randomly oriented needles[15]), 6.3 (horizontal and vertical needles[10]), 5.8 (randomly oriented needles[16]), and 6.56 (horizontal and vertical needles[16]). The fairly small differences between these values can be attributed to statistics (in all cases), finite resolution (for the lattice model), and to the expected small differences in percolation thresholds between completely randomly oriented objects and objects randomly oriented in two orthogonal directions.[2,10] It should be kept in mind that the results in Refs. 10, 15, and 16 were for small systems (unit cell length to needle length was 20 or less), so that finite-size effects must also be taken into account. Also, periodic boundary conditions were not used in Refs. 15 and 16.

For the horizontal and vertical needle problem, we have made a much higher accuracy determination of $n_cL_{\text{eff}}^2$ using the same method as Yonezawa, Sakamoto, and Hori.[17] This involves an examination of the percolation probabilities for increasing system sizes and average, intersection, and union probabilities. The percolation concentration is plotted against $L^{-1/\nu}$ in the usual finite-size scaling manner, where $\nu=\frac{4}{3}$. For averages over 1000 samples, of up to 80 000 needles, we found that $x_c=n_cL^2=6.205\pm0.006$. Note from Table I that $n_cL_{\text{eff}}^2$ does approach 6.2 from below for horizontal and vertical needles, even in the less accurate data from II. The randomly oriented ellipse data in Table II do not show a

TABLE I. This table lists the aspect ratios b/a, $x_I=n_IL_{\text{eff}}^2$, $x_c=n_cL_{\text{eff}}^2$, $n_I\langle a_{\text{ex}}\rangle$, and $n_c\langle a_{\text{ex}}\rangle$ for randomly centered ellipses, oriented in the horizontal and vertical directions, using data taken from II.

b/a	$n_IL_{\text{eff}}^2$	$n_cL_{\text{eff}}^2$	n_Ia_{ex}	n_ca_{ex}
1.0	2.55	5.6	2.00	4.4
0.9	2.55	5.6	2.00	4.4
0.8	2.55	5.7	2.00	4.4
0.7	2.55	5.6	1.98	4.3
0.6	2.55	5.7	1.97	4.3
0.5	2.55	5.6	1.93	4.3
0.4	2.55	5.6	1.90	4.2
0.3333	2.55	5.5	1.85	4.0
0.25	2.55	5.6	1.78	3.9
0.20	2.55	5.7	1.72	3.9
0.15	2.55	5.5	1.65	3.5
0.10	2.55	5.9	1.55	3.6
0.0667	2.55	5.6	1.47	3.2
0.05	2.55	5.6	1.43	3.2
0.04	2.55	5.7	1.40	3.1
0.0333	2.55	5.9	1.38	3.2
0.025	2.55	5.9	1.35	3.1
0.0125	2.55	6.0	1.31	3.1
0.005	2.55	6.2	1.29	3.1

TABLE II. Same as Table I, except for ellipses that were randomly oriented in all directions. The data is taken from II.

b/a	$n_IL_{\text{eff}}^2$	n_cL_{eff}	n_Ia_{ex}	n_ca_{ex}
1.0	2.55	5.6	2.00	4.4
0.9	2.55	5.6	2.00	4.4
0.8	2.55	5.7	2.00	4.4
0.7	2.55	5.8	1.98	4.5
0.6	2.55	5.8	1.97	4.5
0.5	2.55	5.6	1.94	4.3
0.4	2.55	5.6	1.91	4.2
0.3333	2.55	5.6	1.88	4.1
0.25	2.55	5.5	1.83	4.0
0.20	2.55	5.7	1.80	4.0
0.15	2.55	5.4	1.76	4.0
0.10	2.55	5.5	1.71	3.7
0.0667	2.55	5.3	1.68	3.7
0.05	2.55	5.4	1.67	3.5
0.04	2.55	5.4	1.66	3.5
0.0333	2.55	5.5	1.65	3.5
0.025	2.55	5.5	1.64	3.5
0.0125	2.55	5.5	1.63	3.5
0.005	2.55	5.5	1.63	3.5

similar rise in the needle limit. This higher value of x_c may then be an artifact due to having only two orientations.

IV. REANALYSIS OF ELLIPSE RESULTS AND NEW INVARIANT

The success of the normalized variable[10,16] $x=nL_{\rm eff}^2$, in unifying the two sets of data shown in Fig. 2 led us to reanalyze the data in II on the percolation thresholds of sheets with random elliptical holes. The value of $L_{\rm eff}$ for an ellipse with semimajor and semiminor axes a and b, respectively, is defined by combining Eqs. (3) and (4):

$$L_{\rm eff}=2(a+b)\ . \tag{6}$$

Table I shows the results for ellipses that were only allowed to lie in the horizontal and vertical directions, and Table II shows the results for randomly oriented ellipses. The numbers in the column marked $x_I=n_IL_{\rm eff}^2$ are the same, because the exact value of the initial slope for this problem was used to define $L_{\rm eff}$. Within error bars of ± 0.2, the value of x_c seems to be invariant with respect to the ellipse aspect ratio. The third and fourth columns show n_I and n_c, made dimensionless by multiplying with the excluded area,[9,18] $a_{\rm ex}$. In these columns there is clearly a monotonic decrease in the values as the aspect ratio of the ellipses decreases, while in the x_c column there seems to be only random scatter about an average value of about 5.7 in Table I, and about 5.5 in Table II, with the aforementioned small but significant rise in the needle limit in Table I.

It therefore appears that the area defined by $L_{\rm eff}^2$ leads to a better invariant than does the excluded area $a_{\rm ex}$. The quantity $L_{\rm eff}^2$ is designed to lead to an invariant initial slope x_I. However, the constancy of x_c was not expected a priori, but is dramatically demonstrated in Tables I and II.

Figure 3 shows simulation[12] and experimental[19,20] conductivity data for randomly centered circles, replotted using the variable $x=n_cL_{\rm eff}^2$, where $L_{\rm eff}$ for a circle is given by (6) to be twice the diameter. The solid line is the same universal curve as that plotted in Fig. 2 for the needle data, and agrees with the simulation data very well and with the experimental data fairly well.

In II it was shown that p_c for the data in Tables I and II was a good fit to the formula

$$p_c=(1+4y)/(19+4y)\ , \tag{7}$$

where $y=b/a+a/b$. However, we find that p_c can be equally well fitted to the relation

$$p_c=(\tfrac{1}{3})^{4/(2+y)} \tag{8}$$

as shown in Fig. 4. This is important to the present discussion, because using $p_c=\exp(-\pi abn_c)$ together with (8) implies that

$$x_c=n_cL_{\rm eff}^2=16\ln(3)/\pi=5.60 \tag{9}$$

is a universal value for all aspect ratios b/a. Using the initial slope variable $x_I=n_IL_{\rm eff}^2$, along with Eqs. (6) and (9), leads to $x_c/x_I=2\ln 3=2.20$ for all ellipses. The only exception is for horizontal and vertical needles where x_c rises to 6.2 from 5.6 as was noted earlier.

V. DEFECTS WITH ARBITRARY SHAPES

A. Digital-image method

The success of the new invariant for ellipses of arbitrary aspect ratio led us to speculate that this new invariant might hold for randomly centered holes of completely arbitrary shape. To be able to simulate percolation-conduction problems involving such shapes, one is forced to go to a lattice or digital-image approach.

We consider two kinds of shapes. The first are shapes made up of combinations of needles, which are represented in the same way as were the single needles, by removing conducting bonds on a square lattice.

Objects with finite area, like squares or ellipses or more

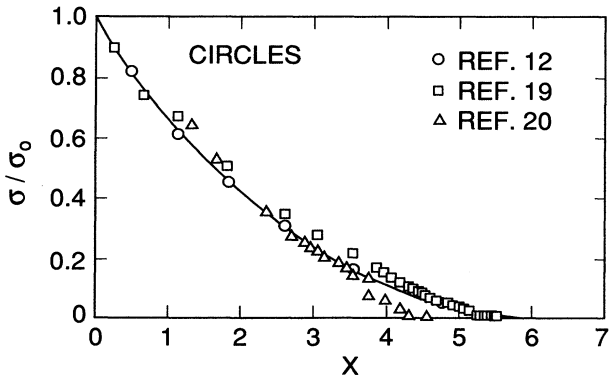

FIG. 3. Showing the conductivity vs $x=nL_{\rm eff}^2$ data for circles. The circles are from the blind-ant algorithm,[12] the squares are the experimental results of Lobb and Forrester,[19] and the triangles are the experimental results of Sofo *et al.*[20] The solid line is the universal conductivity curve (15).

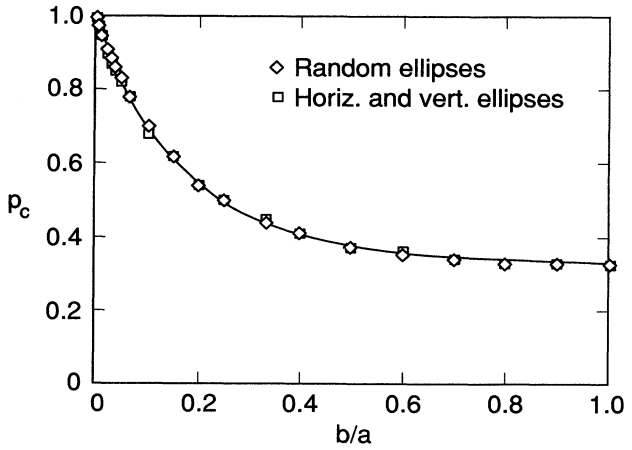

FIG. 4. Showing the percolation threshold p_c vs aspect ratio b/a for the problem of randomly centered elliptical holes. The data points are from Table I, and the solid line is Eq. (8).

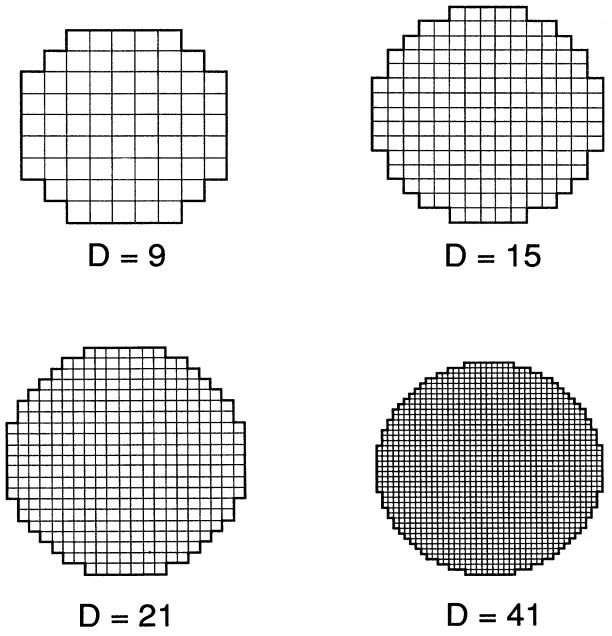

FIG. 5. Showing a series of circles represented by an increasing number of square pixels arranged on a square lattice. The accuracy of the representation increases with the number of pixels used.

unusual shapes, are represented using digital-image techniques,[21] using square lattices of square pixels. Figure 5 shows a series of circles represented by pixels. The circles were generated by centering a continuum circle, with a diameter D ($D=9,15,21,41$) set to an odd number of pixels, on a given pixel. Other pixels were then included in the digital-image representation if their *centers* fell inside the radius of the continuum circle.[21] It is somewhat surprising, but encouraging, to note that for diameters of 15 pixels or greater, the area of the digitized circle as determined by the number of pixels included in the circle by the above construction agrees with the area of the continuum circle $\pi D^2/4$ to within less than 1%.

After a digital image is created, say of randomly centered insulating ellipses oriented in the horizontal and vertical directions, one-pixel-wide electrodes are "glued" on opposite sides, and a conductor network is created with nodes at the center of each pixel. Figure 6 shows the resulting conductor network superimposed on an example of a random image. Conductors with conductance $\Sigma_{i,j}$ connect nearest-neighbor pixels i and j, which themselves have conductivities σ_i and σ_j. The conductance $\Sigma_{i,j}$ is defined as the series combination of Σ_i and Σ_j:

$$\Sigma_{i,j}=\left[\Sigma_i^{-1}+\Sigma_j^{-1}\right]^{-1}, \tag{10}$$

where Σ_i is the conductance of one-half of pixel i. This means that $\Sigma_i=2\sigma_i$. If pixels i and j are both conductors with conductivity σ_0, then $\Sigma_{i,j}=\sigma_0$. If either pixel i or

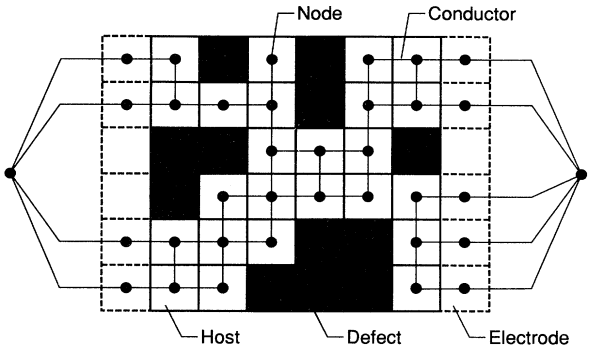

FIG. 6. Showing an example of a digital image with random conducting and insulating regions, along with one-pixel-wide electrodes attached to the ends. The network of conductors into which the image is mapped is also shown, superimposed onto the image.

pixel j represent insulating materials, then $\Sigma_{i,j}=0$. The last case of interest is if pixel i is on the electrode, and pixel j has finite conductivity σ_j. The electrodes are considered to have infinite conductivity, which results in the value of $\Sigma_{i,j}$ being $2\sigma_j$.

B. Test cases

We wish to demonstrate, beyond the needle problem discussed above, that this lattice approach to continuum problems gives accurate results in cases where n_I and n_c are known from a true continuum analysis. We give one test case for n_I, and three for n_c.

The test case for n_I that we consider involves elliptical defects with semimajor axis a and semiminor axis b, placed in a conducting matrix, as described in Sec. IV. The exact solution for the effect on the conductivity of a single defect was given in Eq. (1), but is rewritten here in a slightly different form. The change in conductivity in an $N\times N$ (all lengths in units of pixels or lattice spacing) sheet with host conductivity σ_0 is given, using Eq. (1), by

$$\begin{aligned}\delta\sigma^H/\sigma_0 &\equiv 1-\sigma^H/\sigma_0=\pi b(a+b)/N^2\ ,\\ \delta\sigma^V/\sigma_0 &\equiv 1-\sigma^V/\sigma_0=\pi a(a+b)/N^2\end{aligned} \tag{11}$$

when the defect is insulating, and H and V again stand for horizontal and vertical orientation of the ellipse with respect to the horizontally applied voltage.

For $N=200$, $a=21$, and $b=9$, the calculated values of $\delta\sigma^H/\sigma_0$ and $\delta\sigma^V/\sigma_0$ differ from the exact values by an average 7.2%. The same percentage difference was obtained for an $N=400$ pixel lattice, so that this disagreement was not due to the ratio a/N being too small, which would be a finite-size effect, but rather must be caused by the finite resolution of the conductor-insulator boundary. To confirm this, another computation was done using $N=400$, $a=45$, and $b=19$, which gives approximately the same aspect ratio hole as in the previous case, but with twice the resolution. This time the relative error for $\delta\sigma^H/\sigma_0$ and $\delta\sigma^V/\sigma_0$ was cut in half, to 3.6%, denoting a boundary effect. We expect that the percentage error in

$\delta\sigma^H$ and $\delta\sigma^V$ goes to zero linearly with the number of pixels used per unit length of the ellipse. We note that, as in the case of the lattice needle, digitized ellipses always cause a greater reduction in the conductivity than would be expected from Eq. (11). The ellipses could be represented reasonably well, electrically, by an effective continuum ellipse, with $a_{\text{eff}}=a+0.5$, and $b_{\text{eff}}=b+0.5$. Since no electrical connection is made between a boundary defect pixel and a boundary host pixel, electrically the defect appears slightly bigger than its geometric size.

Computing an accurate value of n_c would seem to be more problematical than computing n_I, since the percolation threshold is determined by tortuous, thin paths of connected material. These paths will certainly be affected by the finite resolution, in the sense that the minimum path thickness is limited to be one pixel, or $1/N$ in terms of the system size N. Fortunately, there are three (at least) true continuum computations of critical thresholds against which the digital-image techniques can be compared.

The percolation threshold of randomly centered, overlapping circles has been much studied.[6,15,22] Reference 6 lists a number of values for p_c based on various independent computations, which range from a high of 0.38 to a low of 0.31, with the best estimate probably being about 0.32. Using a 1000×1000 lattice, our results for p_c are 0.35 ± 0.02 (21-pixel-diam circles), and 0.33 ± 0.02 (41-pixel-diam circles). For either size circle, the critical threshold results are within 10% or less of the best estimate for p_c. The value of p_c was determined by using a burning algorithm[3] to check for continuity in both directions for 20 configurations, and taking the average of the p_c's computed for left-right and up-down percolation over 20 configurations.[17]

Dubson and Garland have experimentally measured the critical threshold for randomly placed, overlapping parallel squares,[23] and found a rather high value of $p_c=0.39\pm0.01$. Pike and Seager[15] did a continuum simulation of the same problem, and found $p_c=0.33$. Gawlinski and Redner also obtained[24] $p_c=0.33$. Our value, obtained using 20×20 squares placed on a 1000×1000 lattice, is $p_c=0.35\pm0.02$.

The final comparison case is the dependence of p_c on the aspect ratio of randomly placed, overlapping ellipses, the problem discussed in Sec. III. The continuum analysis carried out in II was for randomly oriented ellipses and for ellipses that were only oriented in the x and y directions. The lattice results, obtained on 500×500 lattices with ellipses all having $2a=41$ pixels and various aspect ratios b/a, although not shown here, reproduce the two-orientation ellipse continuum results shown in Fig. 3 within the computational uncertainty.

Having demonstrated the kind of accuracy to be expected from our digital-image simulations, we proceed to study the values of n_I and n_c for a collection of arbitrary shapes.

C. Results

Figure 7 shows the 11 shapes studied, seven of which are shapes defined by collections of needles, and four of which are shapes defined by collections of pixels. Each shape was studied on a 1000×1000 (1000×999 for the needle shapes) lattice, and the longest dimension of each shape was either 20 bonds long for the needle shapes, or 20 or 21 pixels long for the pixel shapes. The values of n_i (suitably averaged over orientation) and n_c were computed for each shape. The quantity L_{eff} was defined via Eq. (4), using the computed value of n_I.

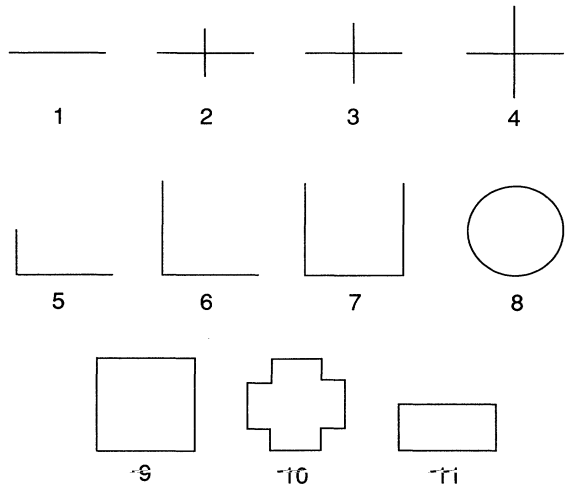

FIG. 7. Showing the various shapes that were used in this paper to study the relationship between n_c and n_I. The numbering scheme is the same as that used in Table III.

Table III shows the results for n_I, n_c, and $n_cL_{\text{eff}}^2$. With the exception of shape Nos. 3 and 4, the quantity

$$n_cL_{\text{eff}}^2=(8/\pi)x_c/x_I=5.9 \tag{12}$$

is invariant to within 5% or less, for needle shapes and for solid pixel shapes. The corresponding values for shape Nos. 3 and 4 are still within 30% of this number, however. Equation (12) should hold up under a true continuum analysis, as the lattice method would be expected to underestimate *both* n_I and n_c, as was discussed above, and so the ratio might well be unaffected.

We have also checked the invariance of x_c for com-

TABLE III. This table lists the values of n_c, n_I, and $x_c=n_cL_{\text{eff}}^2$, for all shapes studied digitally. Here $L_{\text{eff}}^2=8/\pi n_I$. The numbering scheme follows that given in Fig. 7.

Shape no.	n_c	n_I	x_c
1	0.0133	0.0060	5.7±0.2
2	0.0114	0.0047	6.2±0.2
3	0.0098	0.0036	6.9±0.3
4	0.0089	0.0030	7.6±0.3
5	0.0079	0.0034	5.9±0.3
6	0.0047	0.0020	6.1±0.3
7	0.0029	0.0012	5.9±0.4
8	0.0030	0.0014	5.6±0.3
9	0.0026	0.0011	5.9±0.3
10	0.0033	0.0015	5.7±0.2
11	0.0048	0.0021	5.9±0.3

TABLE IV. This table lists the values of $n_c\langle L_{\rm eff}^2\rangle$ for mixtures of two circles, with varying diameter and number ratios. Here $L_{\rm eff}^2=8/(\pi n_I)$.

Diameter ratio	Number ratios 1:1	2:1	3:1
41:31	5.8±0.5	5.8±0.4	5.9±0.4
41:21	6.0±0.4	6.0±0.3	6.0±0.3
41:13	6.0±0.4	5.9±0.3	5.9±0.2
41:9	6.1±0.4	6.1±0.4	6.1±0.4
61:11	5.9±0.5	6.0±0.5	6.1±0.5
81:11	5.8±0.6	5.9±0.6	6.0±0.6
81:9	5.8±0.7	5.8±0.6	5.9±0.6

binations of shapes. Table IV shows the results for different proportions of two sizes of circles, and Table V shows similar results for two sizes of needles. In this case, the quantity $\langle L_{\rm eff}^2\rangle$ is used to normalize n_c, where $\langle L_{\rm eff}^2\rangle$ is averaged over the relative number concentrations of the two different size objects. The first column in both tables is the ratio of large to small diameter or needle length, and the next three columns contain the results for $n_c\langle L_{\rm eff}^2\rangle$ for 1:1, 2:1, and 3:1 ratios of the number of small objects to the number of large objects. In both cases, it is clear that $n_c\langle L_{\rm eff}^2\rangle$ is the same for these cases, within 5 or 10%. There is some effect of the ratio of unit cell to needle length in Table V, as the results for the 20:4 needle length ratio are somewhat different from those for the 40:8 needle length ratio. This could also be due to statistics, as there are fewer of the larger needles used, since the unit cell was always 1000×1000 lattice spacings.

We have obtained one final result, for a system where 41-pixel-diam circles and three times as many 40-lattice-spacing-long needles were simultaneously mixed. The value for x_c ws 5.6±0.3, invariant within computational uncertainty, so that this invariant also holds for mixtures of different shapes, as well as for collections of the same shape.

VI. DISCUSSION

From the results reported in the previous sections, it appears that the quantity $x_c=n_cL_{\rm eff}^2$ is a constant, suggesting that the conductivity $\sigma(x)$ may be a universal function of $x=nL_{\rm eff}^2$. Given our larger data base, it seems appropriate to improve on the two interpolation formulas (A) and (B) given in I, in order to develop an analytical form for this universal function. Denoting these two formulas by $\sigma_{\rm A}$ and $\sigma_{\rm B}$, we form an improved interpolation formula σ as

$$\sigma^{1/t}=\alpha\sigma_{\rm A}^{1/t}+(1-\alpha)\sigma_{\rm B}^{1/t}\,, \tag{13}$$

where $0<\alpha<1$ is an adjustable parameter. The result (13) may be written as

$$\frac{\sigma}{\sigma_0}=\left[\left[1-\frac{n}{n_c}\right]\left[1+\frac{n}{n_c}+\frac{\alpha n^2(tn_I-n_c)}{t^2n_I^2n_c}\right]\Big/\left[1+\frac{n}{n_I}\right]\right]^t$$
$$=\left[\left[1-\frac{x}{x_c}\right]\left[1+\frac{x}{x_c}+\frac{\alpha x^2(tx_I-x_c)}{t^2x_I^2x_c}\right]\Big/\left[1+\frac{x}{x_I}\right]\right]^t, \tag{14}$$

TABLE V. This table lists the values of $n_c\langle L_{\rm eff}^2\rangle$ for mixtures of two needles, with varying length and number ratios. Here $L_{\rm eff}^2=8/(\pi n_I)$.

Length ratio	Number ratios 1:1	2:1	3:1
20:4	5.7±0.2	5.7±0.2	5.7±0.2
20:6	5.7±0.2	5.7±0.2	5.7±0.2
20:8	5.6±0.2	5.6±0.2	5.6±0.2
20:10	5.7±0.2	5.6±0.2	5.6±0.2
20:14	5.6±0.2	5.7±0.2	5.6±0.2
40:10	6.0±0.4	5.9±0.4	6.0±0.4
40:6	6.0±0.4	5.9±0.4	5.9±0.4
40:4	6.0±0.4	6.0±0.4	5.9±0.4
40:2	6.0±0.4	6.0±0.5	6.0±0.5
40:8	6.0±0.5	6.0±0.4	5.9±0.3
30:2	5.8±0.3	5.9±0.3	5.9±0.3

where the critical exponent $t=1.30$ for all geometries in two dimensions.[13] The quantity $x_I=n_I L_{\rm eff}^2=8/\pi$ and so we must choose x_c and α. In I, it was suggested on the basis of Eq. (7) that $x_c=18/\pi=5.73$. However, Eq. (8) suggests that $x_c=5.60$ is an equally good fit. Examination of Tables III and IV suggests a value of $x_c=5.9$ would be most appropriate overall, and we adopt this value. The value of α is adjusted to optimize the fits in Figs. 2 and 8, to give $\alpha=0.7$. This leads to a universal conductivity curve for holes in two dimensions,

$$\frac{\sigma}{\sigma_0}=\left[\left(1-\frac{x}{5.90}\right)\times\left(1+\frac{x}{5.90}-\frac{x^2}{24.97}\right)\Big/\left(1+\frac{x}{3.31}\right)\right]^t, \quad (15)$$

where $x=nL_{\rm eff}^2$. For ellipses, $L_{\rm eff}=2(a+b)$, and so it is straightforward to plot the data for needles and circles against the universal conductivity curve as shown in Figs. 2 and 3. The agreement is clearly excellent. We have held all the parameters fixed in (14) and varied x_c, in order to check the dependence on x_c. The quality of the overall fit is insensitive to small changes in x_c for values in the range $5.6<x_c<6.2$.

Figure 8 collects together the experimental data on squares[23] with random centers and rectangular slits[1] with an aspect ratio of about 50:1, also with random centers and oriented horizontally and vertically. Ellipses that are oriented horizontally and vertically, or randomly, represent the only defect shape for which $L_{\rm eff}$ is known in closed form. There is therefore an unknown scale factor for the abscissa in Fig. 8, since we do not analytically know the scale factor between n_c and x_c.

For the slit data, we used careful measurements of the initial slopes S_H and S_V from I, where H denotes all horizontal and V denotes all vertical slits, respectively, to give $L_{\rm eff}$ via

$$\frac{S_H+S_V}{2}=\frac{1}{n_I}=\frac{\pi L_{\rm eff}^2}{8}, \quad (16)$$

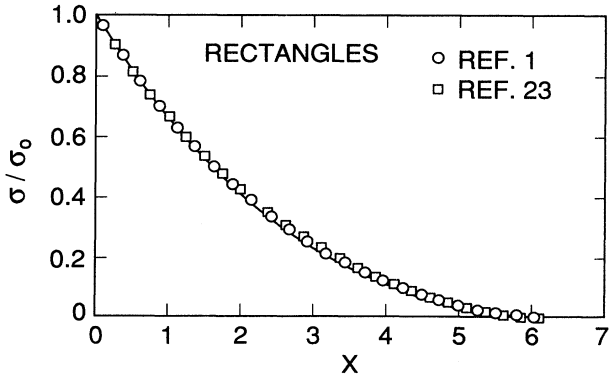

FIG. 8. Showing the experimental results for squares (Ref. 23) and slits (Ref. 1). The solid line is the universal conductivity curve (15).

which is equivalent to fitting the measured initial slope to that of the universal conductivity curve (15) as was done in I. As was shown in I, the slits can be replaced by an ellipse of the same area and same length, $2a=L$. This implies that the aspect ratio b/a of the equivalent ellipse is larger than the aspect ratio w/L of the slit by a factor $\pi/4$, as found within the error bars in Eqs. (6) and (7) of I.

For the square data, we adopted a slightly different procedure and chose the scaling parameter for the abscissa so that the critical points exactly coincided. We fit the critical point to give $x_c=5.9=(28\,440)L_{\rm eff}^2$, where $n_c=28\,440$.[23] This leads to $L_{\rm eff}^{-1}=69.4$. Using the result[15] that the percolation number concentration is the same for squares and circles of equal area, and the result (6) that $L_{\rm eff}=2D$ for a circle of diameter D, we find that the size of the square L is given by $L^{-1}=4/\sqrt{\pi}L_{\rm eff}=157$. This is rather smaller than the (corrected) value of $L^{-1}=172\pm2$ given by Dubson and Garland.[23,25] We feel that the value of $L^{-1}=157$ is more accurate than the value of 172, because it leads to a $p_c=\exp(-n_c l^2)=0.31$, in better agreement with other authors' values[15,24] of 0.33.[26]

The quality of the overall agreement in Fig. 8 is comparable to Figs. 2 and 3. In practice, it makes little difference if $L_{\rm eff}$ is chosen by adjusting the initial slope, the critical point, or the overall fit.

VII. SUMMARY

We have presented an invariant quantity derived from the percolation threshold in terms of the number of defects per unit area n_c and a length $L_{\rm eff}$, which is defined by the change in electrical conductivity caused by a single insulating defect when placed in a conducting host. This invariant has been tested only in problems where the defects are randomly centered and overlapping. It is very important that the variable be the number of defects and not the area fraction remaining p. These are related in a nonlinear way by $p=\exp(-nA)$, where A is the area of a single defect.

Using values of $x_I=n_I L_{\rm eff}^2=8/\pi=2.55$ and $x_c=n_c L_{\rm eff}^2=5.9$, and optimizing a shape parameter $\alpha=0.7$, leads to the universal conductivity curve given in Eq. (15), with $x=nL_{\rm eff}^2$. This applies when the anisotropic holes are aligned horizontally and vertically, or isotropically, to make the conductivity σ isotropic. In general $L_{\rm eff}$ is not known analytically and must be obtained by aligning the horizontal axes of the experimental and universal conductivity curves. This is a straightforward procedure, as x is linearly proportional to the number of inclusions n. In this case, $L_{\rm eff}$ is treated as a fitting parameter. In a few cases, we have more information about $L_{\rm eff}$ from the dilute limit. For ellipses, $L_{\rm eff}=2(a+b)$ where a and b are the semimajor and semiminor axes, respectively. This case has been fully discussed in I and also in this paper. For all other shapes, no exact solutions to the single inclusion problem exist. For squares, it

appears as if there is an equivalence to circles of the same area,[15] so that $L_{\text{eff}}=4s/\sqrt{\pi}$, where s is the edge length of the square. On the other hand, in I, it was shown that a long thin $w\times L$ rectangle behaved electrically as an ellipse with the same area, with major axis $2a=L$, so that $L_{\text{eff}}=L+4w/\pi$. We have found no simple way to generalize these rules to arbitrary shapes, despite some effort. In general, the most we can say is that $L_{\text{eff}}=\beta L$, where L is the maximum spanning diameter of the object, and β is a constant of order 1.

ACKNOWLEDGMENTS

One of us (A.R.D.) would like to acknowledge support from the Center for Fundamental Materials Research. M.F.T. would like to acknowledge support from the National Institute for Standards and Technology. The research at Michigan State has been supported by the Research Excellence Fund from the State of Michigan. We would like to thank M. A. Dubson, C. J. Lobb, and J. Tobochnik for useful conversations and for supplying data in digital form.

[1]Jan Tobochnik, M. A. Dubson, M. L. Wilson, and M. F. Thorpe, Phys. Rev. A **40**, 5370 (1989).

[2]W. Xia and M. F. Thorpe, Phys. Rev. A **38**, 2650 (1988).

[3]Dietrich Stauffer, *Introduction to Percolation Theory* (Taylor and Francis, London, 1985).

[4]H. Scher and R. Zallen, J. Chem. Phys. **53**, 3759 (1970).

[5]R. Zallen, *The Physics of Amorphous Solids* (Wiley, New York, 1983).

[6]E. T. Gawlinski and H. E. Stanley, J. Phys. A **14**, L291 (1981).

[7]D. P. Bentz and E. J. Garboczi, in *Proceedings of the Symposium on Physical Phenomena in Granular Materials,* edited by G. D. Cody, T. H. Geballe, and Ping Sheng (Materials Research Society, Pittsburgh, 1990), Vol. 195, p. 523.

[8]D. P. Bentz and E. J. Garboczi (Cem. Concr. Res. **21**, 325 (1991).

[9]I. Balberg, C. H. Anderson, S. Alexander, and N. Wagner, Phys. Rev. B **30**, 3933 (1984).

[10]I. Balberg, Phys. Rev. B **31**, 4053 (1985).

[11]L. M. Schwartz and J. R. Banavar, Phys. Rev. B **39**, 11965 (1989).

[12]Jan Tobochnik, David Laing, and Gary Wilson, Phys. Rev. A **41**, 3052 (1990); J. Tobochnik, Comput. Phys. **4**, 181 (1990).

[13]D. J. Frank and C. J. Lobb, Phys. Rev. B **37**, 302 (1988).

[14]S. Kirkpatrick, Phys. Rev. Lett. **27**, 1722 (1971); Rev. Mod. Phys. **45**, 574 (1973).

[15]G. E. Pike and C. H. Seager, Phys. Rev. B **10**, 1421 (1974).

[16]P. C. Robinson, J. Phys. A **16**, 605 (1983).

[17]Fumiko Yonezawa, Shoichi Sakamoto, and Motoo Hori, Phys. Rev. B **40**, 636 (1989).

[18]L. Onsager, Ann. N. Y. Acad. Sci. **51**, 627 (1949).

[19]C. J. Lobb and M. G. Forrester, Phys. Rev. B **35**, 1899 (1987).

[20]J. Sofo, J. Lorenzana, and E. N. Martinez, Phys. Rev. B **36**, 3960 (1987).

[21]K. R. Castleman, *Digital Image Processing* (Prentice-Hall, Englewood Cliffs, NJ, 1979).

[22]T. Vicsek and J. Kertesz, J. Phys. A **14**, L31 (1981).

[23]Michael A. Dubson and James C. Garland, Phys. Rev. B **32**, 7621 (1985).

[24]E. T. Gawlinski and S. Redner, J. Phys. A **16**, 1063 (1983).

[25]We are grateful to M. A. Dubson for pointing out that the ratio of the sample size to the square side was quoted in error by a factor of 2 in Ref. 21, and should have been 172 ± 2 rather than 86 ± 1.

[26]It is pointed out by M. A. Dubson that a physical measurement of the area of the squares was not straightforward, and the possibility of a 10% error could not be ruled out.